LIGHTWEIGHT CARBON NANOTUBE CONDUCTOR WITH HIGH ELECTRICAL CONDUCTIVITY AND STABILITY FOR SCALE-UP MANUFACTURING AND POWER TRANSMISSION APPLICATION STUDY

Songlin Zhang, Jin Gyu Park*, Nam Nguyen, Claire Jolowsky, Ayou Hao, and Richard Liang

High-Performance Materials Institute, Florida State University, 2005 Levy Street, Tallahassee, FL 32310, USA, E-mail: jgpark@fsu.edu

Keywords: Carbon nanotubes, Electrical conductivity, Iodine doping, Open air stability, Scale-up production

ABSTRACT

Recently, electrically conductive cables, fibers/wires or tapes of carbon nanotubes have been extensively studied. However, high electrical performance of cables or tapes was focused on the conductive properties of CNT networks with small dimension such as fiber with a diameter around 1-2 μm or tape with a thickness around 500 nm. In this work, a macro CNT sheet was made with large dimension width (around 9 mm) and thickness (around 30 μm). After mechanical stretching, iodine doping and PEDOT:PSS capping, the macro CNT sheet shows high electrical conductivity in the range of 10,000 S/cm (the highest one is around 13,000 S/cm) and this value is stable in open air. Characterizations of SEM, electrical, PPMS and mechanical measurements were conducted. It was found good CNT alignment and high carrier density after iodine doping significantly contributed to the overall high electrical conductivity. The substantial stability of electrical property benefits from the capping layer of PEDOT:PSS which showed little change over 10 days. Additionally, this process is based on commercially available raw materials and scalable for industrial production. This work opens a new path to optimize the conductivity of CNT assemblies with a wide range of engineering applications.

1 INTRODUCTION

Lightweight and corrosion-resistant non-metal electrical conductors are highly desired for applications in aerospace, portable electronics, medical devices and marine instruments [1]. Due to the extraordinary attributes of carbon nanotubes (CNTs), including low density, one dimensional structure, tunable electrical properties and mechanical strength/stiffness exceeding many conductive metals, CNTs have been extensively studied at different scales from nanoscale individual CNTs to macroscale CNT assemblies, such as yarns (also referred to as fibers), sheets (such as buckypaper) or ribbons for electrical conduction applications [2-5]. Although the electrical conductivity of an individual CNT could be as high as 10^6 S/cm for single-walled CNTs (SWNTs) and 3.3×10^4 S/cm for multi-walled CNTs (MWNTs) [6], macroscopic CNT assemblies showed very low conductivity due to the discontinuity, misalignment, loose packing, and impurities, which profoundly impacts the electrons or charge carriers transport due to scattering effect and contact resistance between individual tubes and bundles [4]. A crystal packing structure of CNT assemblies with good alignment leads to a small contact resistance and facilitates the charge carriers transferring among individual nanotubes, and bundles of CNT networks of sizable CNT sheets and tapes [7].

To date, CNT fibers have demonstrated better electrical performance than CNT sheets, which may possibly be due to improved alignment and contacts in CNT fibers with small diameters compared to the relatively large dimensions of CNT sheets. This scale-up issue has attracted attention from many research groups. Zhao et al.[3] reported double-walled nanotube-based fibers assembled by floating catalyst chemical vapor deposition (FCCVD) method, which demonstrated a high electrical conductivity ~20,000 S/cm, with an average density 0.33 g/cm^3, and a diameter ~5 μm. Behabtu et al.[5] successfully spun highly conductive SWNT-based fibers from chlorosulfonic acid assisted CNT dispersion by wet-spinning method. The conductivity for the as-spun fibers was 29,000 ± 3000 S/cm, with a diameter around 10 μm.

However, for engineering applications of large sized CNT sheets, the electrical conductivity has been much lower than that of CNT fibers. When the thickness of the sheet increased from a nanometer scale to a micrometer scale, or even to a millimeter scale, the electrical conductivity was significantly reduced from ~10^4 S/cm to ~10^2 S/cm. For example, Chen et al. reported a vacuum-assisted buckypaper via conjugated cross-linking that exhibited a conductivity around 6,200 S/cm at a thickness of 10-20 μm [8]. Similar results were observed in Laird et al.'s work for polymer single crystal-decorated buckypaper, possessing a conductivity of 1,930 S/cm with a thickness range of 5-20 μm [9]. CNT sheets with a larger thickness of ~60 μm, reported by Zhang et al. [10], exhibited relatively low electrical conductivity of 300 S/cm. This dimension effect on the electrical conductivity of macroscopic CNT assemblies was also observed by Truong et al. [11] and Tran et al. [12]. They concluded that dense packing of CNTs with small dimensions induced by mechanical pressing was a promising method to achieve high performance CNT assemblies.

In our previous work, high CNT alignment and large CNT sheets, produced using a mechanical stretching method, vastly improved the electrical conductivity [13]. Electrical conductivity increased from 420 S/cm (unstretched CNT sheets) to 600 S/cm in the CNT sheets with a 40% stretch ratio. Furthermore, by combining mechanical stretching and hot-pressing, we also observed crystal packing of CNTs in highly aligned CNT reinforced composites [14, 15]. An alignment fraction of up to 0.93 was achieved with a high density packing of the flattened CNTs in the nanocomposites and led to high conductivity. Post-treatments including rolling, pressing and stretching are effective ways to achieve denser packing and improved alignment microstructures of CNT assemblies, and thus resulting in substantially improved electrical conductivity.

Surface functionalization is also another effective route for improving mechanical and electrical transport properties of CNT materials, such as microwave [16], plasma [17], electron beam treatment [18] and chemical functionalization [19, 20]. Among those methods, chemical doping was reported as a promising way to greatly enhance the electrical conductivity of macroscale assemblies of CNTs, including oxidant chemicals such as I_2 [3, 5, 21], ICl [22] and $SOCl_2$ [23]. Iodine, as an important chemical dopant, was reported to achieve metallization of CNT thin sheets by gas phase iodination [21] and even improved the electrical properties of CNT fibers to ~ 67,000 S/cm after doping. The electrical conductivity of wet-spun CNT fibers (diameter around 10μm) doped by chlorosulfonic acid was reported to be further improved to 50,000 ± 5,000 S/cm by iodine doping [5]. A high specific conductivity of 1.24 $S \cdot m^2/g$ was achieved by a p-doping of iodine monochloride [22]. However, such reported samples were at a very small dimension scale.

The high reactivity of oxidant chemicals, including I_2, $SOCl_2$ and HNO_3, resulted in poor air stability, possibly due to the interactions of oxidant chemicals with air and H_2O. Wu et al.[24] reported a de-doping process of iodine from doped graphene through a simple method of immersing in DI water with 30 seconds sonication. Instability of oxidant chemical doped CNTs was also reported by Jackson et al. [25], who coated a polymer layer on the doped sample to minimize this issue of instability, but the absolute value of electrical conductivity was still relatively low.

In this research, we achieved high electrical conductivity in the range of ~10^4 S/cm of highly aligned and doped long CNT sheets for potential applications of lightweight CNT conductors. By using a mechanical stretching method, high CNT alignment was achieved with a dense packing structure, and the electrical conductivity was further improved by iodine vapor doping. This high electrically conductive CNT sheets were fabricated by combining mechanical stretching, iodine doping and a polymer coating layer, which significantly improved the stability of highly conductive sheets. We demonstrated the samples of much large sizes (>1 mm in width) compared to the results from literature (~ 10 μm in width). The capability to produce such sizable material samples is important to accelerate engineering application studies.

2 MATERIALS AND EXPERIMENTS

2.1 MATERIALS AND CONDUCTIVE CNT SHEETS PREPARATION

Carbon nanotube sheets were purchased from Nanocomp Technologies Inc. (NH, USA). Aligned carbon nanotube sheets were prepared using a continuous mechanical stretching method [26]. The details can be found in our previous articles [14, 15]. Due to the high aspect ratio of CNTs (~100,000, based on

~1 mm in length and ~3-8 nm in diameter) [13], the stretching ratio can achieve ~35% for aligned CNT sheets. Stretching ratio is defined as the stretched length subtracted from the original length divided by the original length. In this work, the stretching ratio was controlled at 35% to ensure the structure integrity and promising electrical conductivity. The final products of 35% aligned CNT sheets were measured at 7 mm in width and up to 10-feet in length.

Doping of iodine (purchased from Sigma-Aldrich Inc, St Louis, MO) was conducted in a sealed vial with a fixed iodine concentration. The CNT sheet was placed in the vial at 343 K (70 °C) for several hours. The PEDOT:PSS in water (Sigma-Aldrich Inc, St Louis, MO) was used as received without any dilution. The capping layer of PEDOT:PSS was dip-coated on the surface of CNT sheets and dried at room temperature overnight. Due to the small nanosized pores and hydrophobicity, the capping layer only covered the surface and did not penetrate inside the CNT sheets.

2.2 CHARACTERIZATION

Electrical property measurements were conducted using a current source (Keithley 6221) and nanovoltmeter (Keithley 2182A) in a four-probe configuration. Resistivity (ρ) was calculated from the slope of the I-V curve based on the equation:

$$\rho = R * w * t/d \quad (1)$$

where R is resistance; w, t and d are width, thickness and distance of the sample as shown in Figure 2a. All calculations were based on the assumption of CNT sheets with a rectangular cross-section. Scanning electronic microscope (SEM, JSM-7401F, JEOL.) with EDS for elemental mapping was used for morphology analysis. TEM images and elemental mapping from energy-filtered TEM were taken using the JEM-ARM200cF (JEOL) at 80 kV with GIF camera (Gatan). Raman analysis was done by a Renishaw inVia micro-Raman system using a 785 nm excitation wavelength. Thermogravimetric analysis (TGA) before and after doping was conducted in a Q50 (TA Instrument Inc.) with a 10 °C/min heating rate in air. Temperature dependent electrical resistivity was measured using a conventional four-probe method from 300 K down to 4 K using physical properties measurement system (PPMS, Quantum Design).

2. RESULTS AND DISCUSSION

2.1. ELECTRICAL CONDUCTIVITY IMPROVED BY MECHANICAL STRETCHING

2.1.1. IMPROVEMENT ON ALIGNMENT BY MECHANICAL STRETCHING

Carbon nanotube alignment from nanoscale to macroscale is significantly crucial to preserve the excellent properties of individual CNTs to macro assemblies including CNT fibers (yarns), strips/ribbons and sheets/films (buckypaper) for various range of applications. A simple mechanical stretching method following our previous research[15] was applied to effectively transform random CNT networks into highly aligned ones in this work, as seen in Figure 1a. After stretching, the iodine doped CNT sheets can be done by vapor doping in a confined vial and then stabilized by a capping layer of conductive polymer Poly(3,4-ethylenedioxythiophene)-poly(styrenesulfonate) (PEDOT:PSS) through a feasible dip-coating method. In this research, the pristine CNT sheets, comprised of randomly oriented CNT networks, were stretched to achieve high alignment of the CNTs. Through a continuous stretching method, an aligned CNT sheet of various lengths and widths can be manufactured by adjusting the width and length of the random CNT sheets. For this work, 1-inch-wide of random CNT sheets up to 8 feet in length was used. Figure 1b-c shows SEM micrographs of random and stretched CNT sheets. The small CNT bundles with entanglement, waviness and several-hundred-nanometer and microscale pores were randomly oriented as shown in Figure 1b. By applying mechanical stretching, the entangled CNTs became aligned along the stretching direction (Figure 1c) to form an ordered structure with larger bundles and denser CNT packing, and confirmed by the bulk densities of 0.67 ± 0.07 g/cm^3 and 0.91 ± 0.04 g/cm^3 for random and stretched CNTs, respectively. Figure 1d shows the image of meters-long aligned CNT sheets on a spindle.

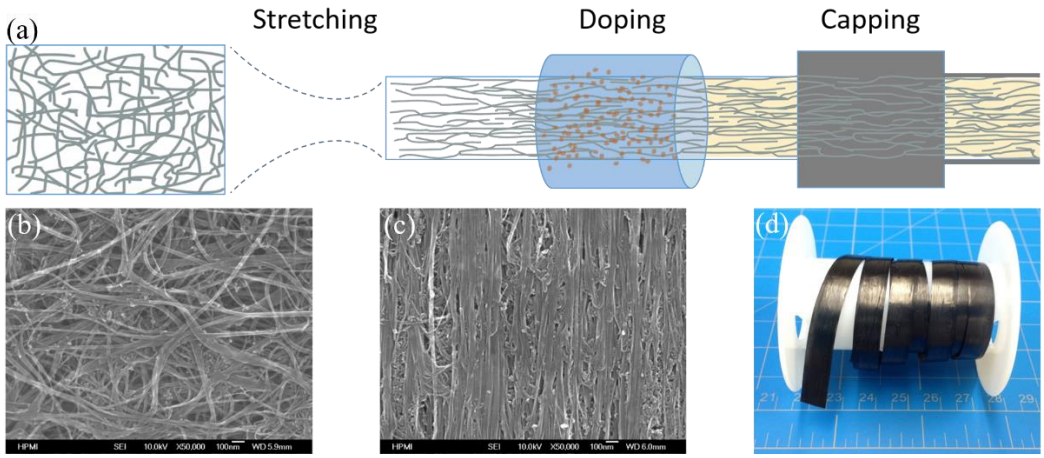

Figure 1: (a) Schematic illustration for the fabrication of highly conductive and macroscopic CNT sheets, including mechanical stretching, chemical doping, and dip-coating (stabilization) processes. (b) and (c) SEM images of CNT networks for random one (b) and stretched one. (d) Digital image of meters-long aligned CNT sheets on a spindle.

2.1.2. EFFECTS OF ALIGNMENT ON CONDUCTIVITY

Mechanical stretching is an effective and simple way to facilitate CNT alignment along the stretching direction for entangled CNT networks of long nanotubes [13, 14]. In this study, the electrical conductivity of CNT sheets with different stretch ratios were tested by a four-probe configuration method (Fig. 2a) to demonstrate the structure-property relationships after stretching (Fig. 2b). As the stretching ratio increased from 0% to 40%, the electrical conductivity gradually increased from ~1,000 S/cm of the random samples to ~2,500 S/cm of 40% stretching ratio ones as shown in Figure 2b. No big difference of conductivity between CNT sheets with 35% and 40% stretching ratio was observed. Therefore, random (0%) and 35% stretched CNT sheets were selected for the remainder of the study.

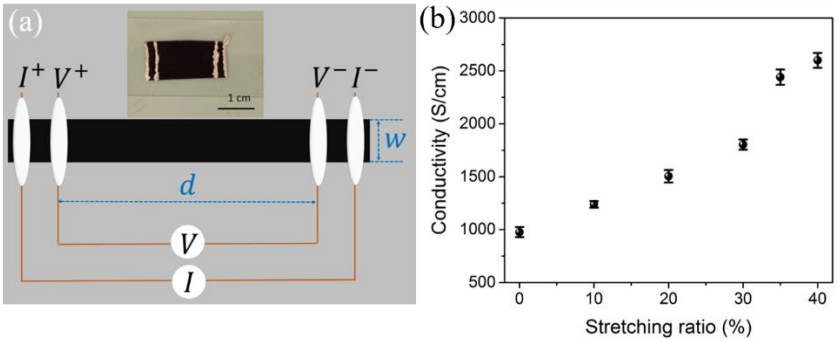

Figure 2: (a) Illustration of four-probe configurations for electrical conductivity test, the inset is the digital image of setup. (b) The relationship between stretching ratio and room temperature electrical conductivity.

Good alignment enhanced the contacts between individual CNTs and bundles, the dense packing structure and even dramatically formed and improved graphitic crystal-like microstructures[15] from the mechanical stretching resulting into a better connectivity and long-range order, hence improved electrical conductivity can be achieved [27]. For the stretched CNT sheets, a significantly improvement of electrical conductivity (σ) was observed at 35% stretching ratio, which were 2.5 times higher than that of random CNT sheets as shown in Figure 2b. In detail, the conductivity increases slowly at the initial stretching stage due to the completely randomly oriented CNTs becoming relative ordered, then increase fast after 20% stretching ratio because the effect of alignment on the electrical conductivity becomes more evident comparing to other parameters such as cavities (or air bubbles) in the macro assemblies. To keep the CNT sheets' structural integrity, the stretching ratio reaches a limitation due to nanotube assemblies breakage beyond what the current nanotube aspect ratio can handle [13].

2.2. EFFECT OF IODINE DOPING ON ELECTRICAL PROPERTIES OF CNT SHEETS

2.2.1. DOPING PROCESS

Iodine doping process was conducted in a sealed vial with a fixed iodine concentration. Iodine became vapor phase from solid and formed small active molecule upon heating. The structure integrity for both random (Fig. 3a) and 35% stretched CNT sheets (Fig. 3b) are preserved after doping, due to the mild doping conditions. Iodine will sublimate at room temperature and the velocity of iodine molecule will increase at high temperature. A higher velocity of iodine molecule helps the penetration into CNT sheets easy and fast. As a result, an improved efficiency of iodine doping was observed as shown in Figure 3c as temperature increased. Higher temperature may cause structural damages to CNT network. In addition, a conductivity plateau was shown as doping time passing by (Fig. 3d). Considering the iodine doping effectiveness and cost effectiveness, a relative low temperature (70°C) and short doping time (3 hours) were applied in this study.

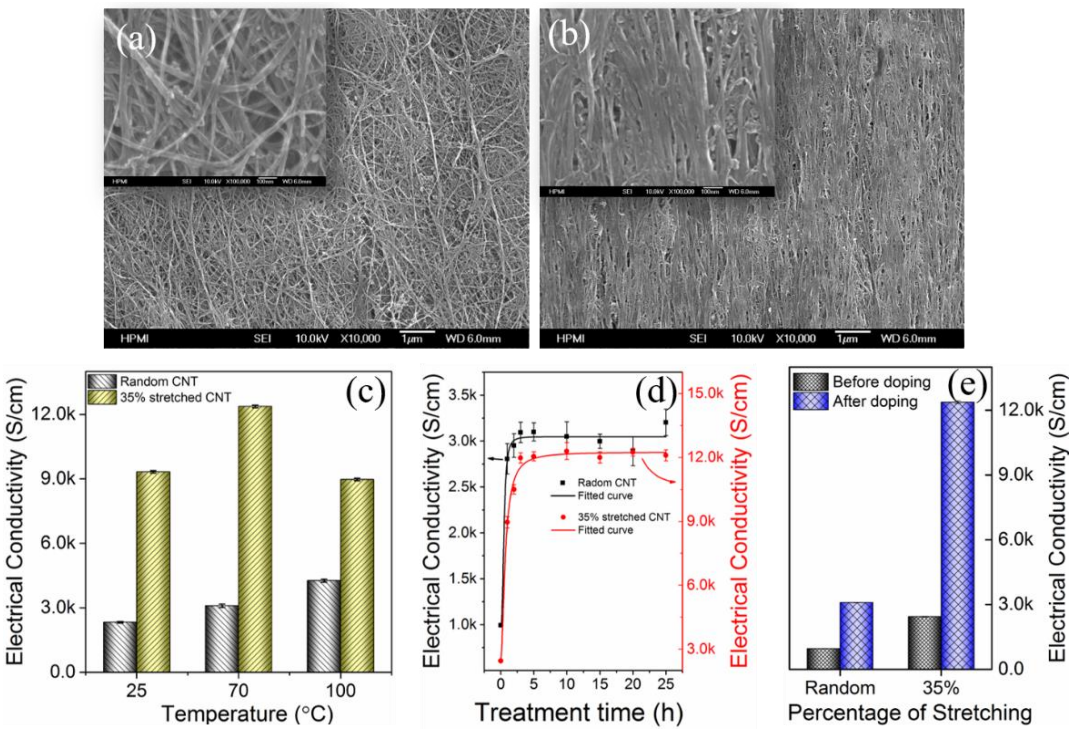

Figure 3: (a) and (b) SEM morphology of random (a) and stretched (b) macroscopic CNT sheets after iodine doping process. (c) Effects of temperature and (d) doping time on the electrical conductivity for both random and 35% stretched CNT sheets. (e) The synergistic effects of mechanical stretching and chemical doping on the room temperature conductivity improvement of macroscopic CNT sheets.

The doped 35% stretched CNT sheets showed a dramatically enhanced electrical conductivity from ~2,400 S/cm to ~12,000 S/cm (Fig. 3e), an improvement of nearly 5 times due to the high electron affinity of iodine, which can facilitate the electron transfer and generate more holes in CNT networks [21]. Compared to the random CNT sheets with electrical conductivity of ~ 1,000 S/cm, the electrical conductivity of doped 35% stretched CNT sheets significantly improved to nearly one magnitude higher. More importantly, this process is highly scalable for realizing both high electrical conductivity and larger size of CNT sheets compared to fibers and thin ribbons reported in recent literature [3, 5, 7, 12], the iodine doped CNT sheets are very attractive for further engineering application studies.

2.2.2. DOPING QUALITY AND MECHANISM

To increase electrical conductivity of CNT assemblies, oxidant chemicals, such as I_2 [21], ICl [22] and $SOCl_2$ [23] are effective dopants. Those dopants are typical electron acceptors to enhance the electron transfer within the CNT networks. Raman spectroscopy results, shown in Figure 4a and the

inset, exhibited several unique peaks related to the iodine doping. An apparent feature peak after doping was observed in Figure 4a at 153 cm^{-1} for doped 35% stretched CNT sheets (not seen in un-doped random or undoped 35% stretched samples), which can be attributed to iodide anion formation of triiodide (I_3^-) and/or pentaiodide (I_5^-) [21, 24]. There was an up-shift in the G band by 4 cm^{-1} from 1583 cm^{-1} to 1587 cm^{-1} for doped 35% stretched CNT sheets in Figure 4a inset, compared to undoped random and 35% stretched samples, which had the same peaks at 1583 cm^{-1}. This apparent shift towards larger wave numbers from iodine p-doping, was attributed to the charge transfer between CNTs and polyiodine [21]. A higher value of the red shift in the G band indicated a higher doping level of CNTs, which resulted from not only doping on the surface CNTs but also doping on the bundles inside of CNT sheets. No significant discrepancies were found in the D band at 1310 cm^{-1} for both random and 35% stretched CNT sheets. While after iodine doping, the intensity of the D band for 35% stretched CNT sheets shows an enhancement, with a higher I_D/I_G ratio indicating more defects in the CNT structure. Zhao et al.[3] reported a covalent bonding between iodine and CNTs, which may explain the induced defects after doping.

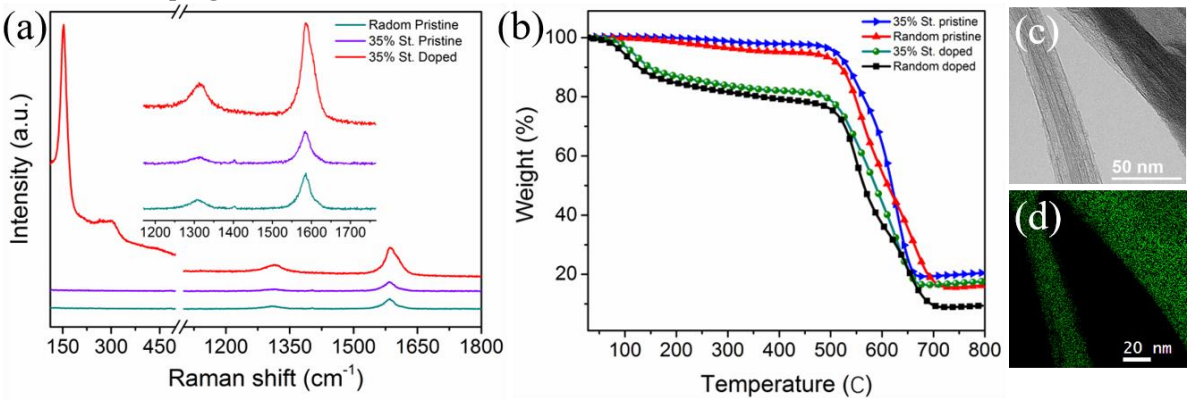

Figure 4: (a) Raman spectroscopy of random and 35% stretched CNT sheets for radial breathing mode (RBM) and D band and G band (inset is a detail of D and G band). (b) TGA analysis of random and 35% stretched CNT sheets before and after iodine doping. (c) TEM image of two CNT bundles at high magnification and (d) their iodine mapping.

Table 1. TGA data of doped random and 35% stretched CNT sheets.

	Iodine (%)	Degradation temperature (ºC)	
		Onset	End
Doped random CNT	13.2 ± 1.7	42.5 ± 2.0	197.9 ± 8.0
Doped 35% stretched CNT	11.0 ± 1.0	41.5 ± 1.7	208.3 ± 3.8

To evaluate the iodine doping quality, thermogravimetric analysis (TGA) was used to evaluate the amount of iodine that was absorbed by the CNT sheets, as shown in Figure 4b. The iodine desorption peak was 105 °C and the random CNT sheets showed a higher iodine percentage of 13.2 wt.%, compared to the 35% stretched CNT sheets of 11.0 wt.%, as shown in Table 1. In our experiments, more than a 10% doping level of iodine was achieved without causing any physical damage to the structure of the CNT assemblies. This demonstrated the effectiveness of vapor phase doping rather than using liquid iodine doping, which necessitates a harsh condition to achieve a high doping level [28]. Moreover, the high doping level also indicated that vapor iodine allowed easy penetration from the surface to the inside of the CNT sheets, possibly due to the porous microstructures of the random and stretched samples [7, 12]. The energy-dispersive X-ray spectroscopy (EDS) was applied to verify the distribution of iodine in random and stretched CNT sheets. As shown in Figure 4c-d, a homogeneous distribution of iodine after doping was observed, indicating that most of the CNT bundles are uniformly covered by iodine (Figure 4d). This verified that iodine was not only deposited on the surface but also penetrated inside the random and stretched CNT networks due to their porous nature and vapor phase doping process.

2.2.3. DISCUSSIONS ON DOPING MECHANISM

As an oxidant chemical, iodine was expected to increase electrical conductivity by hole doping [21]. The hole concentration (n) of iodine doped sample, as shown in Table 2, was calculated from the measured Hall coefficient (R_H) according to the equation:

$$R_H = -\frac{1}{ne} \tag{2}$$

where e is the electron charge. Based on hole concentration and hole mobility, the electrical conductivity (σ) is defined by:

$$\sigma = ne\mu \tag{3}$$

where μ is the hole mobility. After iodine doping, the hole concentrations of random and 35% stretched samples are 2.90×10^{19} cm^{-3} and 2.67×10^{19} cm^{-3}, respectively, which are one order of magnitude higher than that of their undoped counterparts (Table 2). The difference in hole concentrations between the doped random and 35% stretched CNT sheets possibly originates from the different iodine doping levels. As shown in Table 1, 13.2 wt. % of iodine was doped on the random CNT sheet samples, higher than 11.0 wt. % of doped 35% stretched one. Furthermore, the doped 35% stretched CNT sheets presented the largest carrier mobility at ~2800 $cm^2/(V\cdot s)$ out of all samples listed in Table 2.

Table 2. Hall measurement of doped CNT sheets.

	Random CNT	Doped random CNT	35% stretched CNT	Doped 35% stretched CNT
Carrier concentration(cm^{-3})	1.65×10^{18}	2.90×10^{19}	1.62×10^{18}	2.67×10^{19}
Carrier mobility ($cm^2/(V\cdot s)$)	959	689	2312	2805

2.3. CONDUCTION MECHANISM OF CNT SHEETS BY IODINE DOPING

To further gain a fundamental understanding into the electrical conduction mechanism of CNT networks, the behavior of conductivity at low temperatures is a useful indicator about metallic or semiconducting behavior regarding different conduction mechanisms as a result of different chemical treatments [29-31]. Therefore, we measured the effects of iodine doping on the temperature dependence of electrical conductivity of CNT samples from 300 K down to 4 K.

Figure 5a shows the temperature dependence of resistivity of random and 35% stretched CNT sheets before and after iodine doping from 300 K down to 4 K. The high conductivity of the CNT sheets at 300 K was retained at low temperature (4 K) for all four samples, extrapolating to a non-zero value in zero temperature limit (Table 3 lists the detailed conductivity values). This feature is an important signature of free charge carriers of metallic behavior [31]. Another metallic conduction behavior that was observed was the positive temperature coefficient of resistance (TCR) from the crossover temperature (T_c, the temperature at resistivity minimum) to near room temperature. These characteristics show a conduction mechanism that is dominantly metallic conduction for doped random and 35% stretched CNT samples in a broad temperature range from the crossover temperatures T_c at 65 K and 46 K, respectively, to 300 K. At the same time, the variation of resistivity after iodine doping was obviously smaller compared to the undoped samples, indicating a relatively weak temperature dependence. However, the small dip in resistivity at the crossover temperature (T_c) was retained and moved to a much lower temperature after iodine doping.

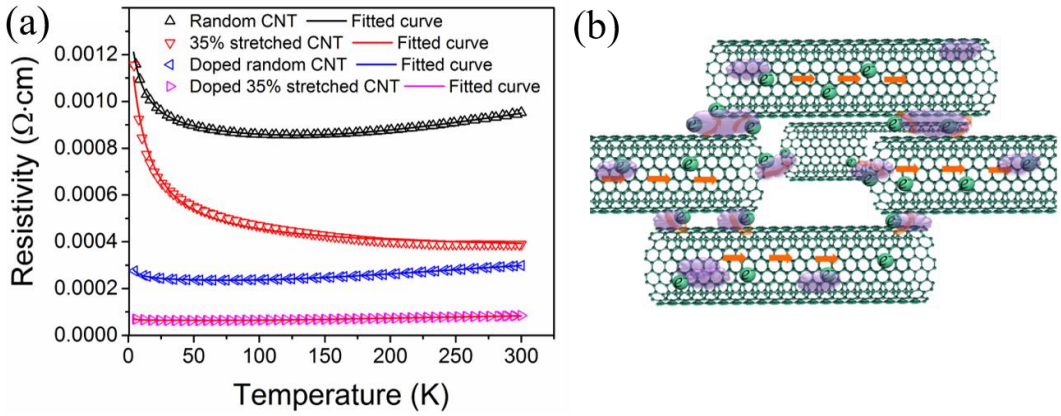

Figure 5: Temperature dependence of resistivity for both random and 35% stretched CNT sheets before and after iodine doping. (a) The absolute resistivity value and the simulated curve based on heterogeneous model. (b) Schematic illustration of electrical conduction mechanism described by heterogeneous model.

Table 3. Electrical resistivity at different temperature.

Resistivity ($\times 10^{-4}$ Ω·cm)	Temperature (K)		
	4	T_c	300
Random CNT	12.16	8.56 (124 K)	9.47
Doped random CNT	2.78	2.36 (65 K)	2.98
35% stretched CNT	11.98	3.81 (247 K)	3.89
Doped 35% stretched CNT	0.704	0.632 (46 K)	0.844

The general conduction behaviors of our samples were similar to the characteristics of temperature dependence of resistivity shown in conducting polymers[29, 30] and in SWNT networks [30-32], which were described by the heterogeneous model [29]. Simply, resistivity of the CNT sheets mainly occurred due to two reasons: the resistance of individual CNTs and the contact resistance between CNTs, arising from electron tunneling through the contact barrier [3, 5, 6, 33]. Tunneling contact barrier induced resistance comes from the gap between CNTs where carriers transfer from one to another nanotube within the same bundle or the nearby one. In CNT networks, carrier transporting barriers are misalignments, twists (waviness), inter-tube or inter-bundle contacts or other defects along the CNTs. Taking into account barrier resistance given by fluctuation-assisted tunneling through thin barrier between metallic regions[34] and the metallic resistance arising from backscattering by phonons along CNT longitudinal direction [30], an expression for the resistivity, described by the heterogeneous model[29] is given by:

$$\rho(T) = \frac{1}{\sigma(T)} = B\ exp\left(\frac{T_b}{T_s+T}\right) + A\ exp\left(-\frac{T_m}{T}\right) \quad (4)$$

where A and B represent the geometrical factors particularly depending on the alignment of nanotubes and bundles of the CNT networks, which can be viewed as constants for specific samples. Typical barrier energies are related with the value of k_BT_b (where k_B is Boltzmann's constant), and the resistivity of quantum tunneling through the barrier in low temperature limit is indicated by the value of factor T_s/T_b. The energy of backscattering phonons is defined by k_BT_m. Figure 5a shows the well fitted curves, and Table 4 lists all the fitted values of the parameters. Since the resistivity minimum moved to a lower temperature after iodine doping, the metallic temperature dependence was dominant and primarily contributed to the temperature-dependent metallic term in Equation (4). As expected, barrier energies k_BT_b between metallic regions increased as resistivity increased. Considering the same magnitude of carrier concentration of doped samples, the smaller value of T_s/T_b in random sample is possibly due to the disorder scattering from the misalignment of nanotubes, suggesting a smaller fraction of delocalized carriers contributed to the conductivity. However, the 35% stretched sample had a higher value of T_s/T_b, indicating that delocalized metallic carriers significantly contributed to the total conductivity [35], which explains the high conductivity because of CNT alignment. The high alignment

and dense packing allow delocalized carriers to transport from one conductive region to another or from one individual CNT to another because of the more compact structure and short junction length [6]. Therefore, the conduction nature of CNT networks after iodine doping was metallic, interrupted by thin barriers through which tunneling occurs.

Table 4. Fitting parameters of heterogeneous model.

	Random CNT	35% stretched CNT	Doped random CNT	Doped 35% stretched CNT
$k_B T_b$ (meV)	0.4848	0.2481	0.1323	0.0484
T_s/T_b	1.828	1.921	2.552	4.363

In addition, Figure 5b illustrates a carrier transferring model of CNT networks. Among all individual CNTs of doped random CNT sheets, the only effective CNT segments that were contained in the conductive path contributed to the electrical conductivity. Carriers go through the shortest conductive path with the lowest contact resistance and shortest junction length between the nanotubes. For the doped 35% stretched CNT case, due to high alignment of individual CNTs and dense structure, carriers went through directly along the nanotubes with a short junction gap between the nanotubes. The synergistic effects of high alignment and dense structure with shorter junction lengths and high carrier concentration resulting from iodine doping, provided the doped 35% stretched CNT sheets a higher electrical conductivity than all other samples.

2.4. OPEN AIR STABILITY AND SIZE EFFECT OF HIGHLY CONDUCTIVE CNT SHEETS

The challenge for chemical doping of CNT by iodine, HNO_3 or $SOCl_2$ [3, 5, 23] is the open air stability even though the electrical conductivity could be significantly improved. In recent work [25, 36], conductive polymers (CPs) was simply used as a coating layer or a component to fabricate CNT/CPs composite materials, which showed no negative effects on the electrical conductivity of the resulting materials. CPs was also reported to strengthen electrical performance to some extent and help stabilize the conductivity under the open air condition [25]. Among the CPs, PEDOT/PSS was widely utilized as a binder to fabricate CNT/PEDOT:PSS composite fiber and film for electrical field application. At the same time, PEDOT/PSS layer was found to possess great potential to preserve the electrical conductivity of CNT film. As a capping layer, PEDOT/PSS thin film would act as a protective shell to avoid the reaction of doping chemicals such as iodine, HNO_3 or $SOCl_2$ with air and also prevent the desorption of dopants from the film.

Figure 6a represents the unstable nature of iodine doped random and 35% stretched CNT sheets and the effects of the coating layer of PEDOT:PSS on the stability of electrical performance of 35% stretched CNT sheets after doping. The doped random and 35% stretched CNT sheets without any coating layer both showed an electrical conductivity decrease of 37% and 28% after 4 days, respectively, due to the unstable nature of iodine and its possible desorption. After the initial 4 days, the conductivity became stable with small fluctuations afterwards. After coating PEDOT:PSS layer on the doped 35% stretched CNT sheets, the electrical conductivity slightly increased and then stabilized at around 104% of the conductivity of the uncoated control samples. There was no conductivity change for testing conducted in open air and room temperature after one week for doped 35% stretched CNT sheets with an additional layer of PEDOT:PSS, indicating its protective shielding effects on avoiding the decrease of electrical conductivity.

Electrical conductivity consistency of different sizes or dimensions of CNT networks must be addressed since CNT sheets of large dimensions are desired instead of ones at the nanoscale size for potential engineering applications. Figure 6b shows the comparison of electrical conductivity of CNT sheets of different dimensions. Normally, the larger the dimensions of the samples, the lower the electrical performance. In our study, when the width of CNT sheets varied from 1 mm to 7 mm, conductivity showed a slight fluctuation at ~10,000 S/cm after iodine doping. Therefore, mechanical stretching combined with iodine doping is a promising way to produce highly conductive CNT sheets with variable large sizes and good conductivity consistency.

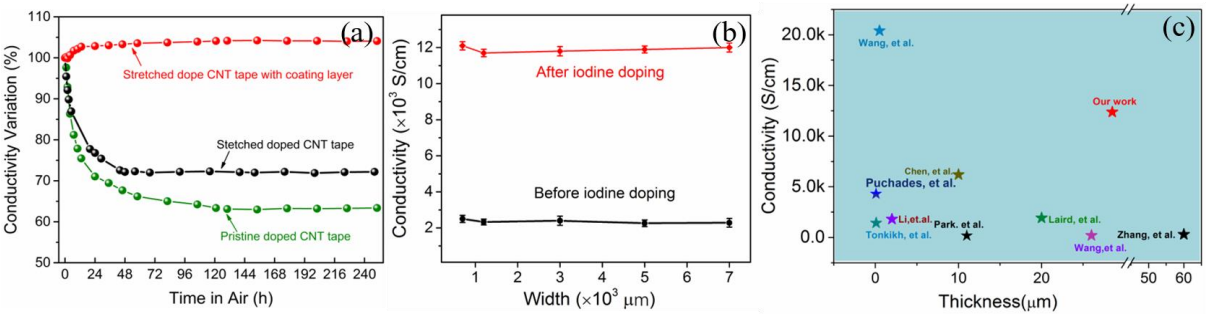

Figure 7: The open-air stability of conductivity and the size effects. (a) Effect of capping layer of PEDOT:PSS on the relative electrical conductivity variation (%) of CNT sheets versus time under open air condition for doped random and doped 35% stretched sheets. (b) Effect of size of macroscopic aligned long CNT sheets on the electrical conductivity. (c) Comparison of our work with others' results from the literature.

Zhao et al.'s[3] and other groups[11, 12] observed the size effects of fibers on the properties of CNTs assemblies. In fact, ultra-high electrical conductivity of CNT assemblies were observed experimentally in others reports with small dimensions for yarns (diameter < 10 μm)[37] and sheets (thickness within a few hundreds of nanometer) [7]. However, macroscopic CNT assemblies showed many defects such as a) end-to-end connections, b) tube-to-tube contacts, c) porous tube-to-tube packing structures, and d) alignment of individual nanotubes, which were critical for electron transfer and load carrying capacity. Statistically, the defect frequency of small dimensional samples was much lower than that of large dimensional samples. This explains why small yarns [3], or thin ribbons[37] (usually with a thickness of less than 500 nm) in literature were reported to show high performance in terms of mechanical and electrical properties.

Figure 6c shows the comparison of conductivity of CNT sheets of different thicknesses. Benefiting from the good alignment and stabilized iodine doping by a capping layer of PEDOT:PSS, our results demonstrated great improvements in the conductivity for macroscopic CNT assemblies. In our study, samples were scaled-up to much larger dimensions using the synergetic effects of mechanical stretching and the iodine doping process. The macroscopic CNT sheets were highly aligned along the stretching direction and produced a densely-packed structure, metallized by iodine doping, which reduced the tube-to-tube contact resistance, increased carrier density, and thus led to a higher electrical conductivity.

3. CONCLUSIONS

CNT sheets of high electrical conductivity with outstanding open air stability were developed through CNT alignment, iodine doping, and a conducting polymer protective layer. Scalable manufacturing can be achieved due to the simple mechanical stretching method and vapor phase doping process. The sample dimensions in this study were in the macroscopic scale (>1 mm in width) compared to other reported work (~ 10 μm in width). High alignment was achieved by mechanical stretching, which promises a high potential to improve electrical conductivity to 2,400 S/cm at a 35% stretching ratio due to high CNT alignment and dense packing structure. Iodine doping further enhanced the electrical conductivity to 12,000 S/cm, almost 5 times, and one magnitude higher than that of undoped 35% stretched CNT sheets and random CNT sheets, respectively. EDS analysis confirmed the uniform doping of iodine through the thickness of the CNT sheets. Metallic conduction mechanism was revealed by studying the temperature-dependence of conductivity behavior of the resultant samples. The conductive polymer coating layer of PEDOT:PSS stabilized the electrical performance at room temperature and showed no change after one week. Therefore, metallic conduction characteristics with scalable manufacturing processes could accelerate the utilization of commercially available raw CNT materials for potential lightweight conductor engineering applications.

ACKNOWLEDGEMENTS

This work was also partially supported by NSF Scalable Nanomanufacturing Program project (SNM 1344672) and AFOSR FA9550-17-1-0005 project. We thank Mr. Frank Allen for critical reviewing of the manuscript;

REFERENCES

[1] N. N. Initiative, National Nanotechnology Initiative Strategic Plan. 2007, December.
[2] T. Ebbesen, H. Lezec, H. Hiura, et al., Electrical-conductivity of individual carbon nanotubes. *Nature*, 1996. **382**(6586): pp. 54-56.
[3] Y. Zhao, J. Wei, R. Vajtai, et al., Iodine doped carbon nanotube cables exceeding specific electrical conductivity of metals. *Sci Rep*, 2011. **1**: pp. 83.
[4] A. Lekawa-Raus, J. Patmore, L. Kurzepa, et al., Electrical Properties of Carbon Nanotube Based Fibers and Their Future Use in Electrical Wiring. *Advanced Functional Materials*, 2014. **24**(24): pp. 3661-3682.
[5] N. Behabtu, C. C. Young, D. E. Tsentalovich, et al., Strong, light, multifunctional fibers of carbon nanotubes with ultrahigh conductivity. *Science*, 2013. **339**(6116): pp. 182-186.
[6] Q. W. Li, Y. Li, X. F. Zhang, et al., Structure-Dependent Electrical Properties of Carbon Nanotube Fibers. *Advanced Materials*, 2007. **19**(20): pp. 3358-3363.
[7] J. N. Wang, X. G. Luo, T. Wu, et al., High-strength carbon nanotube fibre-like ribbon with high ductility and high electrical conductivity. *Nat Commun*, 2014. **5**: pp. 3848.
[8] I. W. Chen, R. Liang, H. Zhao, et al., Highly conductive carbon nanotube buckypapers with improved doping stability via conjugational cross-linking. *Nanotechnology*, 2011. **22**(48): pp. 485708.
[9] E. D. Laird, W. Wang, S. Cheng, et al., Polymer single crystal-decorated superhydrophobic buckypaper with controlled wetting and conductivity. *ACS nano*, 2012. **6**(2): pp. 1204-1213.
[10] X. Zhang, T. Sreekumar, T. Liu, et al., Properties and structure of nitric acid oxidized single wall carbon nanotube films. *The Journal of Physical Chemistry B*, 2004. **108**(42): pp. 16435-16440.
[11] T. K. Truong, Y. Lee, and D. Suh, Multifunctional characterization of carbon nanotube sheets, yarns, and their composites. *Current Applied Physics*, 2016. **16**: pp. 1250-1258.
[12] T. Q. Tran, Z. Fan, P. Liu, et al., Super-strong and highly conductive carbon nanotube ribbons from post-treatment methods. *Carbon*, 2016. **99**: pp. 407-415.
[13] Q. Cheng, J. Bao, J. Park, et al., High Mechanical Performance Composite Conductor: Multi-Walled Carbon Nanotube Sheet/Bismaleimide Nanocomposites. *Advanced Functional Materials*, 2009. **19**(20): pp. 3219-3225.
[14] R. Downes, S. Wang, D. Haldane, et al., Strain-Induced Alignment Mechanisms of Carbon Nanotube Networks. *Advanced Engineering Materials*, 2015. **17**(3): pp. 349-358.
[15] R. D. Downes, A. Hao, J. G. Park, et al., Geometrically constrained self-assembly and crystal packing of flattened and aligned carbon nanotubes. *Carbon*, 2015. **93**: pp. 953-966.
[16] Y. Wang, Z. Iqbal, and S. Mitra, Microwave-induced rapid chemical functionalization of single-walled carbon nanotubes. *Carbon*, 2005. **43**(5): pp. 1015-1020.
[17] C.-H. Tseng, C.-C. Wang, and C.-Y. Chen, Functionalizing carbon nanotubes by plasma modification for the preparation of covalent-integrated epoxy composites. *Chemistry of Materials*, 2007. **19**(2): pp. 308-315.
[18] A. Kis, G. Csanyi, J. P. Salvetat, et al., Reinforcement of single-walled carbon nanotube bundles by intertube bridging. *Nat Mater*, 2004. **3**(3): pp. 153-7.
[19] A. Morelos-Gómez, M. Fujishige, S. Magdalena Vega-Díaz, et al., High electrical conductivity of double-walled carbon nanotube fibers by hydrogen peroxide treatments. *J. Mater. Chem. A*, 2016. **4**(1): pp. 74-82.
[20] I. Puchades, C. C. Lawlor, C. M. Schauerman, et al., Mechanism of chemical doping in electronic-type-separated single wall carbon nanotubes towards high electrical conductivity. *Journal of Materials Chemistry C*, 2015. **3**(39): pp. 10256-10266.
[21] A. Tonkikh, V. Tsebro, E. Obraztsova, et al., Metallization of single-wall carbon nanotube thin films induced by gas phase iodination. *Carbon*, 2015. **94**: pp. 768-774.

[22] D. Janas, A. P. Herman, S. Boncel, et al., Iodine monochloride as a powerful enhancer of electrical conductivity of carbon nanotube wires. *Carbon*, 2014. **73**: pp. 225-233.
[23] U. Dettlaff-Weglikowska, V. Skákalová, R. Graupner, et al., Effect of SOCl2 Treatment on Electrical and Mechanical Properties of Single-Wall Carbon Nanotube Networks. *Journal of the American Chemical Society*, 2005. **127**(14): pp. 5125-5131.
[24] Z. Wu, Y. Han, R. Huang, et al., Semimetallic-to-metallic transition and mobility enhancement enabled by reversible iodine doping of graphene. *Nanoscale*, 2014. **6**(21): pp. 13196-202.
[25] R. Jackson, B. Domercq, R. Jain, et al., Stability of Doped Transparent Carbon Nanotube Electrodes. *Advanced Functional Materials*, 2008. **18**(17): pp. 2548-2554.
[26] G. Horne and Z. Liang, Systems and Methods for Continuous Manufacture of Buckypaper Materials. 2015, Google Patents.
[27] M.-Y. Li, Topological and electrical properties of carbon nanotube networks. 2016, FLORIDA STATE UNIVERSITY.
[28] L. Grigorian, K. Williams, S. Fang, et al., Reversible intercalation of charged iodine chains into carbon nanotube ropes. *Physical review letters*, 1998. **80**(25): pp. 5560.
[29] A. B. Kaiser, Systematic conductivity behavior in conducting polymers: effects of heterogeneous disorder. *Advanced Materials*, 2001. **13**(12-13): pp. 927-941.
[30] A. B. Kaiser, V. Skákalová, and S. Roth, Modelling conduction in carbon nanotube networks with different thickness, chemical treatment and irradiation. *Physica E: Low-dimensional Systems and Nanostructures*, 2008. **40**(7): pp. 2311-2318.
[31] V. Skakalova, A. Kaiser, U. Dettlaff-Weglikowska, et al., Effect of chemical treatment on electrical conductivity, infrared absorption, and Raman spectra of single-walled carbon nanotubes. *The Journal of Physical Chemistry B*, 2005. **109**(15): pp. 7174-7181.
[32] A. Kaiser, G. Düsberg, and S. Roth, Heterogeneous model for conduction in carbon nanotubes. *Physical Review B*, 1998. **57**(3): pp. 1418.
[33] S. p. Badaire, V. Pichot, C. c. Zakri, et al., Correlation of properties with preferred orientation in coagulated and stretch-aligned single-wall carbon nanotubes. *Journal of Applied Physics*, 2004. **96**(12): pp. 7509.
[34] P. Sheng, Fluctuation-induced tunneling conduction in disordered materials. *Physical Review B*, 1980. **21**(6): pp. 2180.
[35] A. B. Kaiser, Electronic transport properties of conducting polymers and carbon nanotubes. *Reports on Progress in Physics*, 2001. **64**(1): pp. 1.
[36] L.-n. Fan and X.-c. Xu, A stable iodine-doped multi-walled carbon nanotube-polypyrrole composite with improved electrical property. *Composites Science and Technology*, 2015. **118**: pp. 264-268.
[37] W. Xu, Y. Chen, H. Zhan, et al., High-Strength Carbon Nanotube Film from Improving Alignment and Densification. *Nano Letters*, 2016. **16**(2): pp. 946-952.